

# Diffraction hardware testbed and model validation

David B. Schaechter\*, Patrick E. Perkins\*\*, Paul V. Mammini\*\*, David A. Swanson\*\*, Christopher W. Tischhauser\*\*, Robert S. Benson\*\*, Torben B. Andersen\*\*, Richard S. Bruner\*\*, Richard I. Fowler\*\*, Kevin T. Morimoto\*\*

Lockheed Martin Advanced Technology Center, Palo Alto, CA USA

Lisa A. Sievers, Jet Propulsion Laboratory and the California Institute of Technology, Pasadena, CA USA

## ABSTRACT

Optical systems, which operate over a wide range of Fresnel numbers, are often times performance-limited by diffraction effects. In order to characterize such effects at the 40-100 picometer level, a diffraction testbed has been built which has the capability of measuring diffraction effects at this level. Concurrently, mathematical diffraction modeling tools have been developed that propagate an input wavefront through an optical train, while retaining amplitude and phase information at a grid resolution sufficient for yielding picometer-resolution diffraction test data. This paper contains a description of this diffraction hardware testbed, the diffraction modeling approach, and a comparison of the modeled and hardware test results, which then serves as validation of the diffraction modeling methodology.

**Keywords:** Diffraction, modeling, interferometry, picometer, heterodyne

## 1. INTRODUCTION

Fig. 1 depicts a solid model of the Space Interferometry Mission (SIM), the first interferometric space scientific mission in a series of NASA Origins Programs. This space observatory uses a triad of interferometric observations of stars to make astrometric measurements at the single digit micro arcsecond level. Such observations are of sufficient quality to infer the existence of earth-size planets orbiting remote stars by detecting the reflex motion of the orbiting motion of these planets on the star. This mapping of likely earth-like planetary systems then forms the basis for compiling a set of targets for future observation missions like Terrestrial Planet Finder (TPF).

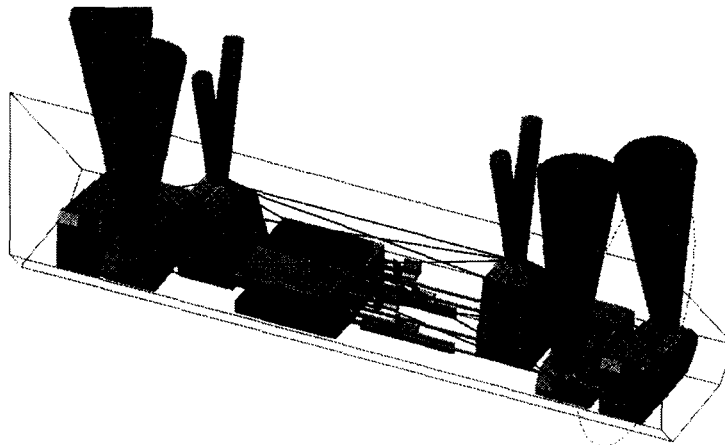


Figure 1: SIM flight conceptual drawing

SIM itself consist of three interferometers. Fig. 2 depicts the operation of one such interferometer. Each interferometer first points its two collecting 35 cm telescopes (separated by a baseline distance of 10 meters) at a target star. Next, an optical delay line using a closed loop control system adjusts the total optical path traversed by the two legs of the interferometer so that the path lengths are equal. Depending on the observation scenario, this delay line may have to make up as much as 2.5 meters of optical path length difference. With an active path length control loop maintaining relative path length difference to the 10-nanometer level, white light interferometric fringes are obtained when the starlight beams are combined. Finally, a precision, sub-aperture 1.06 micron metrology system, which co propagates

\*[david.schaechter@lmco.com](mailto:david.schaechter@lmco.com); phone 650 424-2623; fax 650 424-3106; Lockheed Martin Advanced Technology Center, 3251 Hanover Street B201 OL9-24, Palo Alto, CA, USA 94304. \*\* Lockheed Martin Advanced Technology Center, 3251 Hanover Street B201 OL9-24, Palo Alto, CA, USA 94304.

along the central portion of the star light beam once it enters the SIM instrument, averages a measurement over seconds of observation time to obtain the internal path length traversed by the star light beam to the tens of picometers, which, when combined with the baseline length information, yields the astrometric information of interest.

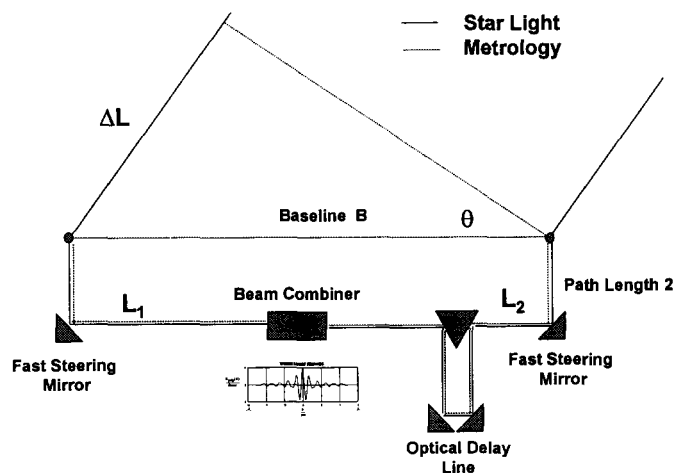


Figure 2: Operation of a White Light Interferometer

In any precision measurement system, one must be diligent in tracking down and minimizing effects of error sources which might corrupt the measurement itself. For SIM, there are many such sources, such as thermal effects, wavefront quality of the optical components, sensor noise, etc. Still another such source of error, and the one which forms the basis for this paper, is the effect of diffraction. In SIM, measurements made at one delay line position setting must be 'combined' in ground processing with those made at a different optical delay line position, and these positions may differ significantly. Because the starlight beams and the metrology beams are of different wavelengths, and different diameters, the beams diffract differently, and the precision metrology system which measures the path length inherits the effects of these diffraction-related errors. Although these effects are only at the several nanometer-level, it behooves the designers, if possible, to first, design SIM in such a way that it is as insensitive as possible to the effects of diffraction, and second, calibrate the residual (repeatable) effects of diffraction to a level which will allow the astrometric measurement of interest to be made at the desired level of precision.

To address the former, a hardware diffraction testbed has been built. It consists of a diffracting element, or mask, that produces a Fresnel number regime characteristic of that in which the SIM flight instrument will operate. The testbed purpose is to produce data which can be used to validate mathematical models of diffraction analysis. The goal of this effort is to devise a diffraction modeling methodology which has been validated at the 40-100 picometer level, with the intent that such a modeling approach can then be used to minimize SIM flight system sensitivity to diffraction effects.

## 2. TESTBED HARDWARE DESCRIPTION

The purpose of the diffraction hardware testbed is to isolate the effects of diffraction, and generate picometer quality data which can then be used to validate the mathematical modeling approach. A block diagram of the system is shown in Fig. 3. The testbed consists of a heterodyne laser system, whose source is a 200 mw, 532 nm solid-state laser. Two acousto-optic modulators (AOMs) form the basis for the heterodyne system. One modulator operates at 80.000 MHz, while the second is tuned to 80.060 MHz, thus setting up a 60 kHz heterodyne signal. The two sources are coupled through single mode fibers to separate 50 mm off axis parabolas which collimate the respective beams.

The signal beam propagates through a diffracting mask, which performs several functions, the primary function being to form a central core beam of a few millimeters diameter, and an outer annular beam of 12-20 mm. These two beams (of different diameters, and thus different Fresnel numbers) then propagate over an optical path, whose path length can be adjusted over a range of 2 meters, thus setting up the capability for examining the difference in diffraction between the two beams as a function of Fresnel number variation. Through the use of two beam splitters, the signal beam is

combined with reference beam, and the annular portion of the combined beams is separated from the central portion of the beam with an annular mirror. The two respective signals are then focused onto detectors which provide signals to a phasemeter which measures the relative phase difference between the core and annular beams, a quantity whose *variation* as a function of path length change is due solely to diffraction.

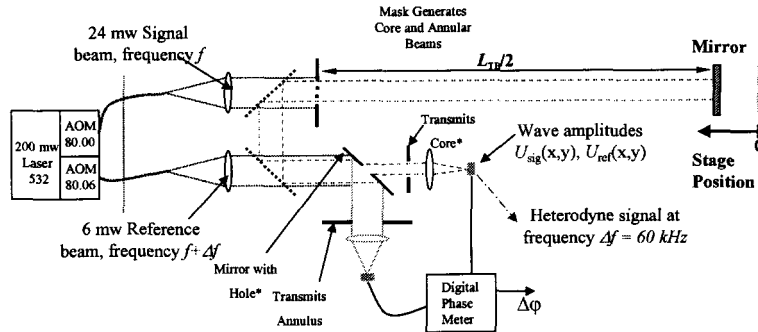


Figure 3: Simplified diffraction testbed block diagram

In reality, the hardware is more sophisticated than that outlined above. The actual testbed hardware, not including the laser source, modulators, phasemeter, control computers and electronics is shown in Fig. 4. The major optical components are four inches clear aperture, and are mounted on Invar tables, and in custom-designed, 300 Hz natural frequency, flexure-supported optical mounts. The fiber feeds to the off-axis parabolas are mounted on a kinematically supported, Zerodur plate in order to present a stable wavefront input to the system, and the main optics are fused silica. The entire assembly, with all of the sensing, alignment, and closed loop controls are vacuum compatible.

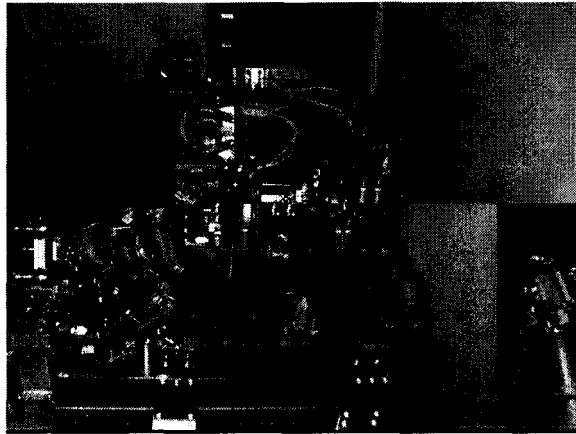


Figure 4: Diffraction testbed hardware

Exquisite care must be taken to isolate the diffraction effects from several, possibly significant, error sources, mainly beamwalk, atmospheric, and thermal. Beamwalk effects are minimized through the use of all fixed, hard-mounted optics with the exception of the 4-inch test article itself, which must translate over a mechanical distance of 1 meter to introduce the path length changes by which the Fresnel number is changed. But herein lies a source of error. A precision, linear stage is used to produce the path length changes, but irregularities in the stage cross track position and tilt as it moves along the stage exceed allowable tolerances. Sub aperture sampling path length errors of 1.6 pm per micron of beam walk are typical of SIM-like optics, so every effort must be made to keep beam walk to a minimum if one desires 40 pm quality data. Requirements for beam walk and tilt control of 2 microns and 100 nanoradians respectively were selected. In order to sense and control the effects of beam walk, the test article is equipped with quad cells.

In the periphery of the 50 mm collimated beam that illuminates the test article (see Fig. 5) through the diffracting mask are two 2-mm beams that register on these detectors. The test article is aligned initially so that the beams are centered on

the quad cells. The test article, mounted on flexures to provide transverse translation capability, is also instrument with 30-nanometer resolution piezomotors that are driven in closed loop control on both transverse axes to maintain this position (i.e. not allow the diffracting beam to walk on its surface) as the test article translates down the stage.

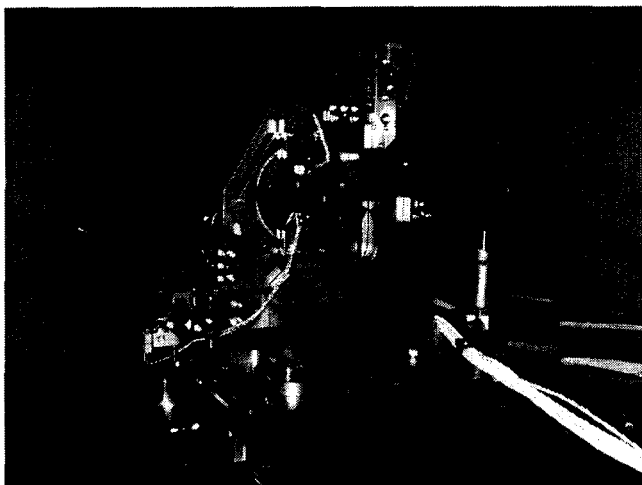


Figure 5: Instrumented test article

Similarly, tilt control of the test article is required so that beamwalk effects on down stream optics is minimized, and so that there is good heterodyne mixing efficiency between the reference and signal beams. The test article itself is equipped with 3 20-micron high voltage piezos which provide the tip-tilt motion. Two sensing schemes, a coarse and a fine, are provided, both of which operate by picking off (with a beam splitter) a portion of the return beam from the test article. The first sensor extracts a portion of the annular beam and focuses it onto a 0.5 mm by 0.5 mm quad cell. Wavefront tilt is detected by means of linear displacement on the quad cell. This system provides coarse tilt sensing capability of 1-2 microradians.

In order to sense tilt to better than 100 nanoradians, four portions of the heterodyne signal, which are generated in the periphery of the diffracting mask, are used in a differential phase detection system (identical to the phase detection system used to measure the diffraction effect itself). In this case, the relative phase, or path length measurements are made between apertures located on the left-right and top-bottom sides of the mask. Differential phase measurements of 1 nanometer, over the 25 mm separation provide tip tilt resolution of 40 nanoradians.

Atmospheric path length fluctuations are minimized by operating the entire system in vacuum. Initially, all the hardware is checked out, in-air, and data is obtained to verify functional performance. However, all of the optically based sensing systems for both control and phase detection are limited by atmospherics. The entire assembly shown in Fig. 4 is mounted on an Invar bench, which is, in turn, supported by rollers. It is designed to be moved easily from its in-air location to the adjacent vacuum chamber which is operated at  $10^{-4}$  torr for final tests.

The testbed operates at room temperature, and individual tests are completed rather quickly. Nonetheless, stable wavefronts and repeatability consideration require stable temperatures. When testing under vacuum conditions, the vacuum chamber is pumped down, and allowed to reach thermal equilibrium over 36 hours. All of the sensing and actuation systems are designed to be low power, but the remaining heat loads are from the stage motor itself, and the camera. The camera is turned on long enough to acquire a sample of the input intensity map, and the stepper motor dissipates power only when operating. Both of these heat sources are located at the far end of the table, well removed from the optics. Furthermore, we monitor temperatures at various locations on the bench using platinum resistive thermometers, which provide readings at the 1 mK level. Temperature changes over the course of most final tests were no more than a few mK.

The phasemeter consists of the detectors, cabling, high-speed 16-bit A/D converters, and a dedicated Mercury processor. The outputs from the core and annular beams are sampled at a rate of 8 samples per heterodyne frequency (480 kHz),

and a narrowly tuned digital filter attenuates sharply (100 db) signal content from outside the 60 kHz carrier frequency band. The relative phase information is extracted from the two signals, and is averaged over 1 sec to produce a single phase output. By driving both channels of inputs with a precision HP frequency reference, it has been shown that the inherent noise limit of the signal is 2.5 picometers  $1\sigma$  rms. There is also a small amount of cross-talk between channels that produces another 5 picometers error. Nonetheless, the system has the capability of extracting phase data of remarkable quality. When coupled with the cabling and optical detectors, some additional noise is added to the system. In-air tests (limited by atmospherics) have shown the end-to-end performance to be 1.4 nanometers  $1\sigma$  rms.

### 3. DIFFRACTING MASKS

The purpose of the testbed is to predict diffraction effects in a SIM-like optical system, i.e. in a system which spans a Fresnel number range comparable to that on SIM. SIM consists of white (400nm – 900nm) light interferometers, as well as sub-aperture 1.3 micron monochromatic metrology systems. Fig. 6. depicts the various Fresnel ranges on SIM. In the conceptual stages of the testbed, it was decided that all of Fresnel regimes could be covered by using a single monochromatic (532 nm) source in the testbed, and allowing the beam diameters and propagation distance to vary to produce the needed Fresnel range. The 1 meter propagation distance was fixed by the availability of precision stages, and this, in turn, fixed the beam diameters that would be used to ~12 mm.

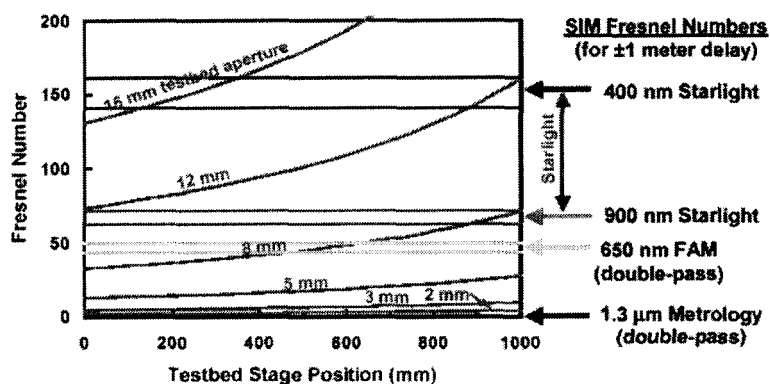


Figure 6: SIM Fresnel number regime

For this testbed, a variety of masks which spanned the needed Fresnel number regime were considered. All of them consisted of a central hole, and an circumscribed outer region consisting of either an annular region or an square 'obscuration'. All of them contained a 'guard band' to reduce mixing of the inner and outer beams due to diffraction. Additional methods of reducing this mixing by separating the two beams in polarization were also considered. Finally, all of the masks contained a set of 100-micron width spiders, this width being selected as large enough to provide the structural support, large enough to be represented in the model, and small enough to diffract a negligible amount of energy into either of the beams. A final consideration in the mask design was that the total laser power in the two beams be matched somewhat to provide for better phase detection.

Fig. 7 Shows the trade space considered for the masks, and highlights those that were selected for testing. The masks were then fabricated using electron discharge machining (EDM), and examined under a microscope for acceptance testing.

Mask	A	B	C	D	E
D Annulus (mm)	12	12	20	20	20
D Obsc (mm)	5	5	8	8	square 8
D Core (mm)	1	2	3	4	3
E(annulus)	0.252	0.252	0.496	0.496	0.213
E(core)	0.0026	0.0105	0.023	0.041	0.023
E(annulus)/E(core)	95.6	24.1	21.2	12	9.1
Max slope (pm/mm)	510	109	73	22	58

Figure 7: Testbed mask trade space

Fig. 8 contains a photograph of mask B, one of the masks under test. The central 2 mm hole, 2-5 mm guard band, the 5-12 mm annulus, and the 100 microns spiders are all visible. Also shown are the alignment pin holes and fastener locations. Other features in the periphery of the mask are the 2 2-mm holes which generate the shear sensing beams used for test article centration, and the 4 5-mm beams which are used by the phase detectors to provide test article tip-tilt sensing information

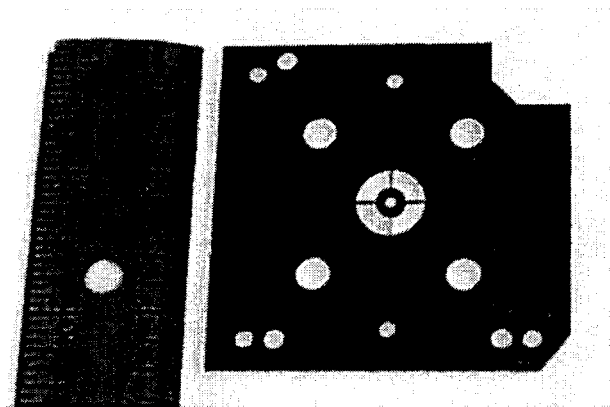


Figure 8: Diffraction testbed mask B

#### 4. ALIGNMENT AND CONTROL

Prior to data taking, the testbed must be carefully aligned, and this alignment must be maintained throughout the data-taking process. The sensing bases for many of the alignment processes are the beam walk and tip/tilt systems discussed earlier. In addition to this, there is also a digital camera that serves several important functions. First, the camera observes both the signal beam and the reference beam. It is important that these two gaussian beams overlap. The 1024 x 1024 Dalsa camera, with its 14-micron size pixel is used to perform this function. Secondly, even though the diffraction models can take an input wavefront and propagate it through the optical system, the phase predictions are sensitive to the shape of the input wavefront itself. The camera provides a digitized map of the intensity profile of the input beams. Finally, the diffracting mask, which generates the core and annular beams, must be located at the center of the gaussian profile, and again, the digital camera provides the capability for centering the mask to sub-pixel resolution.

There are a total of 13 picomotors that provide the ability to (remotely) align the system in tilt and beam walk. There are two such motors on the test article, three more on the fold flat, two on the mask stage, two on the tilt sensor, two on one of the beam splitters, and two on a pupil mask located prior to the annular beam phase detector. The picomotors have 30 nanometer resolution, and sufficient dynamic range to more than meet the testbed needs.

A custom-designed graphical user interface was designed using a Windows-based National Instruments hardware and software system. Its purpose is to monitor and record the stage position, temperatures, test article tip-tilt and beam walk, camera output, and phase meter output. The equipment rack and processor on which it runs also contains all of the digital to analog, analog to digital, frame-grabbers, serial interfaces, high voltage amplifiers, cable interfaces, and controllers needed for the operation of the testbed. The interface supports both a manual mode for initial alignment, as well as a real-time mode for automatically sequencing the entire test and data-taking procedure.

A single test consists of homing the stage, grabbing the input intensity profiles, centering the test article in x-y shear and in tip-tilt, settling, collecting the phase data, recording temperatures, and then moving to the next stage position. Each of the 40 2.5-cm steps requires about 5 seconds for the motion, 15 seconds to center, and a few seconds of integration of phase data, thus completing an entire data-taking set in about 30 minutes.

## 5. MODELING APPROACH

A paraxial wave propagation code, which propagates both the signal and reference beams from element to element, has been written, and checked against some closed-form solutions, where they are available. Nonetheless, the ability of such codes to predict picometer level results in actual hardware, where optic positions, alignment, wavefront, etc are unknown a priori had yet to be proven, and, in fact, is the primary purpose for the existence of the testbed.

The major optical elements in the testbed, such as beamsplitters, are substantially oversized, thus limiting diffraction effects to only the principal optical elements which are included in the modeling. The modeled components include collimating optics, the diffracting mask, any clipping apertures (such as annular mirrors, and pupil masks at the entrance to the detectors), and the detector lenses. No wavefront aberrations, misalignments, or tilt errors were included (except for sensitivity studies), and distances from optic-to-optic were measured only to millimeter accuracy. Heterodyne mixing between the signal and reference beams in the two focal planes then determines the phases in the core and annulus channels. The phase difference, along with the laser wavelength, provides the needed measure of the diffraction optical path difference (the geometric contribution is common to both channels, and cancels).

The wavefronts for modeling the testbed were represented on 1024 x 1024 grids for initial studies. Over the 50 mm beam, this allows for details as small as 50 microns to be resolved in the model, a number that provides some characterization of the 100-micron spiders in the diffracting mask. The model is written in FORTRAN 95, runs on a Pentium IV computer with 2 gigabytes of memory, and requires a few hours to map the phase meter output as a function of test article position at 2.5 mm increments of test article stage position. A typical such result is shown in Fig. 9. It is apparent from this figure that the effects due to diffraction contain significant 'structure', and that the scale of the effect is on the order of 10-20 nanometers.

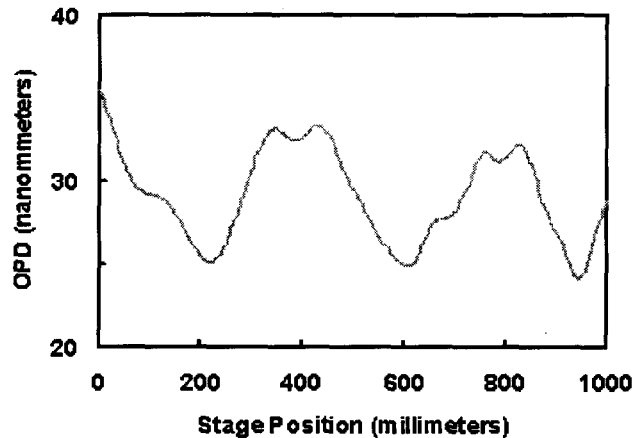


Figure 9: Predicted diffraction model outputs for mask B

To ascertain the ability of this grid resolution to predict diffraction effects at the picometer-level, identical runs of the model at grid resolutions of 1024, 2048, and 4096 were compared. Differences of over 100 picometers in predicted phase output due *solely* to grid resolution demonstrates that the 1024 grid resolution is insufficient for characterizing diffraction effects at the desired level. However, such coarser resolutions are still useful for 'quick' verification that the models and hardware are in step-with one another. All final model results were generated with values that were extrapolated to infinitesimal grid size from the results produced by the 1024-, 2048-, and 4096-grid runs.

## 6. IN-AIR RESULTS

In-air testing, the results of which are captured in Fig. 10, was performed with Mask B. The solid line illustrates the predicted optical path difference (OPD) vs. stage position. The test data, shown with red, green, and blue points, show the results of three repeated tests. Each test begins with the test article at stage position 'zero'. At this stage location,

three relative phase measurements are made between the core and annular beams. Then the test article is advanced 2.5 cm to the next stage position, and again, three phase measurements are taken. One such 'data set', for example the set of red points, is obtained by proceeding over the entire 1-meter stage in 2.5 cm increments, and recording three phase measurements at each location. One such test requires about 45 minutes. Once this data set was collected, the test article was returned to its home position, and a second (green), and then a third (blue) data set were collected.

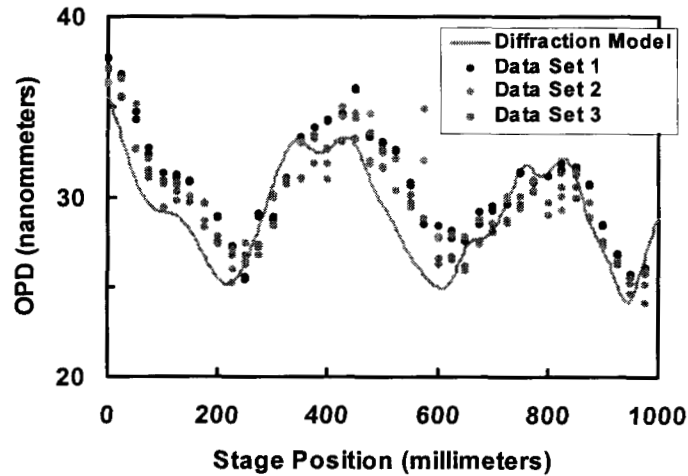


Figure 10: Comparison of model predictions and in-air test data for mask B

The results of this in-air testing confirmed that the model and test results were sufficiently accurate to warrant transitioning the testbed to vacuum operation. The rms noise of the phase measurement system, in air, was determined to be 1.4 nm. At the same time, we obtained that the rms deviation between the model prediction and the test data, averaged over the length of the stage, was 2.0 nm; i.e. the model vs. test agreement was at the noise floor of the in-air measurement capability.

## 7. VACUUM RESULTS

All of the testbed hardware was designed for vacuum compatibility, with the foresight that on a properly designed testbed, atmospherics would be the largest error source in trying to make picometer class measurements. Consequently, the first test performed after transitioning to the vacuum chamber was to characterize the noise floor of the phase measurement on a completely stationary optical system. What we obtained initially is depicted in Fig. 11, and was not encouraging. Just below the in-air noise floor, there appears to be a very low frequency, nanometer-level noise source. The first half Fig. 11 shows the phasemeter output when operating at 50 torr, after which the chamber was pumped down to  $10^{-3}$  torr, and the same character of noise was present at this pressure.

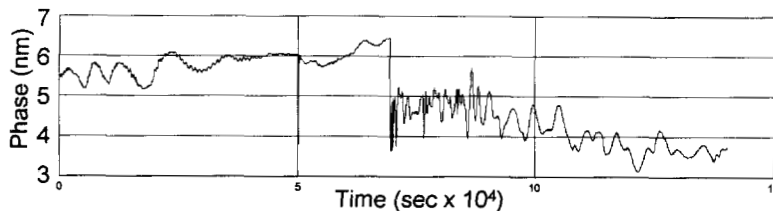


Figure 11: Phase measurement noise under vacuum

After a significant amount of investigative work was expended in tracking down this error source, with no positive results, an alternate data taking method was devised to circumvent the effects of this low frequency disturbance. The

basis for devising a ‘chop’ mode of data taking, as opposed to the in-air method of data-taking which involved moving sequentially from stage position to stage position down the stage track, is contained in Fig. 12.

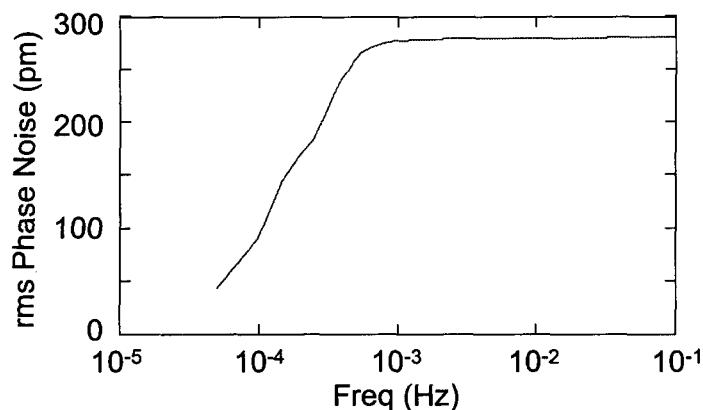


Figure 12: Cumulative power spectrum of phase measurement noise under vacuum

Fig. 12 shows that the bulk of the cumulative rms error from the phase meter occurs at frequencies *below*  $10^{-3}$  Hz. A single, end-to-end test which requires 45 minutes does not provide sufficient immunity from a large portion of this disturbance spectrum. However, if one were able to obtain measurements on a time scale much faster than 1000 seconds, then the contribution from the low frequency measurement disturbance is minimized. The ‘chop’ method for obtaining data exploits this shape of the noise spectrum. For vacuum testing, the revised data taking method is to obtain the change in diffraction path length by making repeated relative phase measurements between adjacent stage positions separated by 2.5 cm, beginning the procedure at stage position zero. Next, the stage is advanced to the 2.5 cm position, and repeated chops are made between the 2.5 cm position and the 5 cm position, thus determining accurately the incremental diffraction phase incurred over this portion of the stage. The benefit of this process is that all of these incremental phase measurements can be made in 20-30 seconds, sufficiently fast to incur insignificant error due to measurement drift.

The results of 101 such chops (typical of all the data taken) for Mask B, taken between stage position 0 cm (green) and stage position 2.5 cm (blue) as a function of time are shown in Fig. 13. The complete data set acquisition time was 1900 seconds, but the time *between* adjacent chops was only 19 seconds. Also visible in Fig. 13 is the noticeable amount of common mode behavior present between the stage 0 cm phase measurement and the stage 2.5 cm phase measurement. Nonetheless, the *difference* between these two curves remains quite steady. In fact, the mean difference between the two chop positions is  $-1.073$  nanometer (this is the amount of phase change due to the incremental diffraction effect over this 2.5 cm segment of the track) and the uncertainty in this mean value, after being measured repeatedly over the 101 chops, is 5.02 picometers, associated with a  $1\sigma$  confidence level. Such results are the basis for claims that incremental diffraction effects are measured to an accuracy of single digit picometers.

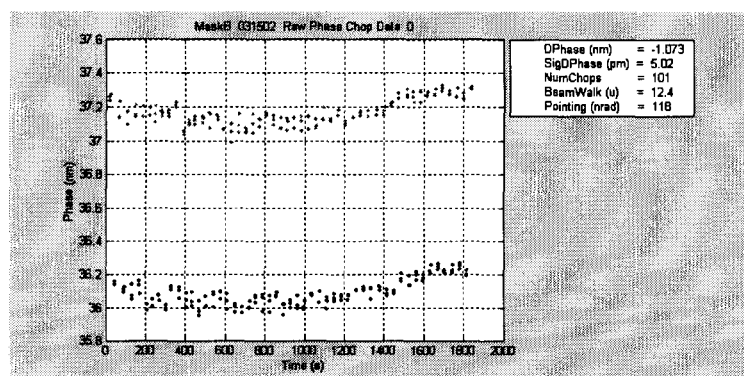


Figure 13: Representative diffraction phase chop data taken for mask B at  $10^{-3}$  torr

One may continue to chop between the 40 adjacent positions over the 1 meter stage length, and record the statistics associated with each station along the track. The results are summarized in Fig. 14. This figure shows that the accuracies to which the 40 incremental phases are determined vary from just a few picometers to as large as 26 picometers, and that the mean uncertainty over the entire length of the stage is 14 picometers.

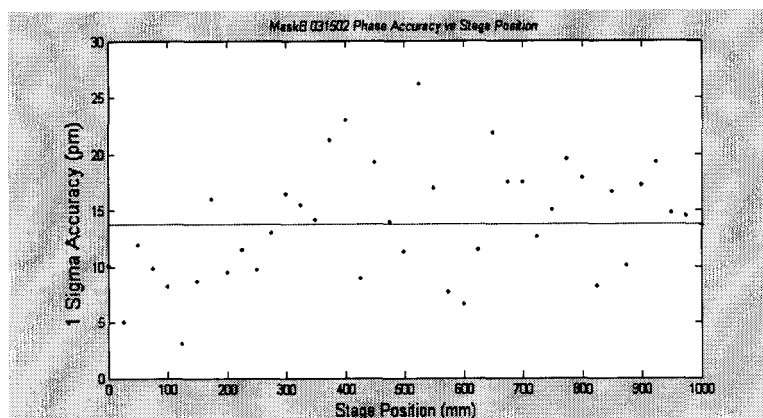


Figure 14: Mask B incremental phase data accuracy over the 1 meter stage length

Once all of the incremental diffraction phase measurements are obtained, they may be ‘pieced together’ or ‘integrated’ from start to end to produce the entire diffraction phase vs. stage position curve analogous to Fig. 10. These results (plus some additional ones) are shown in Fig. 15. First, the solid black line represents the model results. Next, the blue line shows the integrated incremental results, which are supposed to agree with the model results. Third, the red points show test data that was taken in the original sequential way, starting at stage position 0 cm, and proceeding (not chopping) down the stage to the 30 cm position. A similar such partial plot is shown in green and corresponds to the end-of-the-stage sequential data acquisition. Finally, the cyan ‘smear’ consists of moving the stage to a fixed position at 42.5 cm, staying there, and recording 3600 consecutive phase measurements over the period of 1 hour.

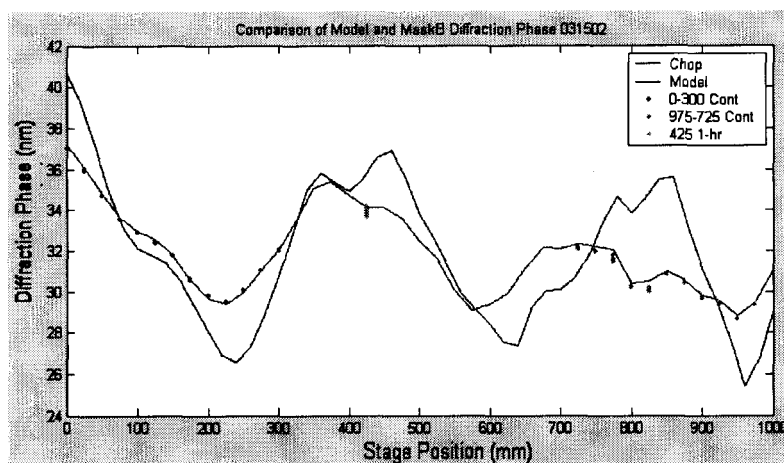


Figure 15: Mask B final results

An interpretation of these results follows. First, we have already observed with Fig. 14 that the ‘error bars’ associated with the test data are on the order of a few picometers, too small to be shown on this plot. The fact that the red, green, and cyan points track the test data, even though they were obtained many hours after the chop data, speaks for the repeatability and stability of the test results. The smear of the cyan dots reflects the prior observation that there is a low frequency drift in the measurement system that can produce a drift over the course of this single 1 hour data set that is on

the order of several hundred picometers. Finally, agreement between the model predictions and the vacuum test data was somewhat poorer than expected, and in fact, *not* as good as the results obtained in air and shown in Fig. 10.

Again, some investigative work ensued, and, with the aid of the model itself, produced the following likely explanation for the poorer agreement between model and test data. When the optical testbed was moved from its in-air location to the vacuum location, we believe that the aperture mask for the core channel (shown in Fig. 3) was likely misaligned. If one hypothesizes lateral shift of this aperture, and uses the model to produce a series of diffraction phase curves for various decentration values, one obtains the results in Fig. 16. With this as a guide, it is reasonable to believe that the in-air test results match the properly aligned (red) curve (to 2.0 nm rms), while the vacuum test data best matches the blue curve (to 414 pm rms) which corresponds to a mask offset of 100 microns.

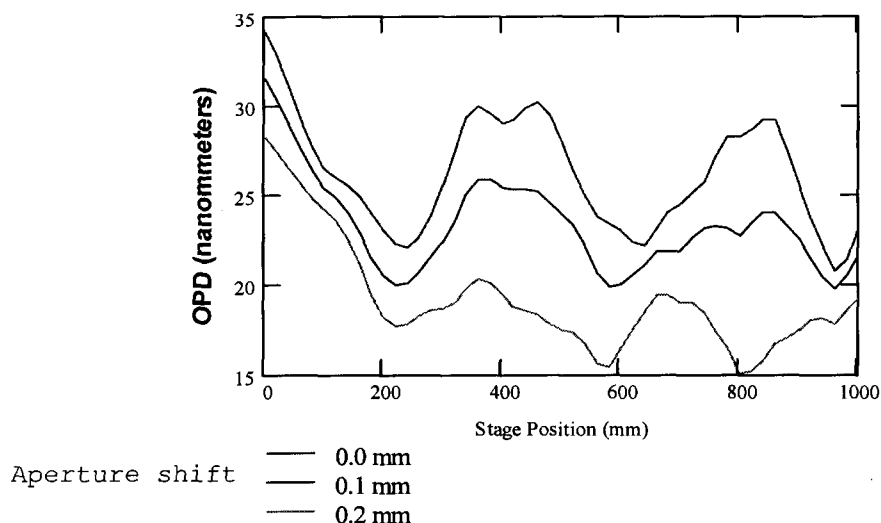


Figure 16: Mask B model predictions as a function of core beam detector aperture decentration

By the time the Mask B test data had been analyzed fully, the testbed had already been removed from the vacuum chamber, Mask B had been unmounted, and the testbed was being reconfigured to run with Mask C. With knowledge of the sensitivity to this core mask alignment, extra effort was devoted to properly aligning the Mask C testbed. Three other modifications based on Mask B test results were also implemented:

- to allow for an additional 10 seconds of pointing control loop settling time prior to acquiring the chop data. This still provided immunity from the low frequency measurement noise error, but increased data taking time from 6 hours to 8 hours for a complete data set
- to more carefully align the linear stage translational axis with the optical axis signal beam, thus reducing the amount of beamwalk in the system
- to change the number of chops at each stage position. It was deemed that 21 chops at each stage position were sufficient to achieve the desired performance levels

With these modifications in hand, and with in-air checkout for the Mask C configuration producing noise floor limited agreement between models and test data, Mask C vacuum tests were initiated. The significant results of these tests are captured in below. Fig. 17 shows the agreement between the Mask C test data and the model results, assuming in the model no core mask offset. The agreement between the raw test data and the model prediction is 432 pm rms over the length of the stage. If one accounts again for a possible mask offset, the agreement improves to 262 pm rms.

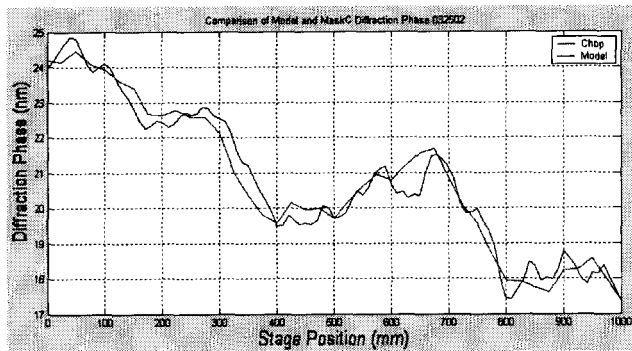


Figure 17: Mask C model predictions agree with test data to better than 432 picometers rms.

Evidently, the extra effort taken in aligning the Mask C testbed, the allowance for extra settling time, and the fact that Mask C is inherently less sensitive to alignment proved beneficial. The error bars associated with the test data of Fig. 17 decrease to 6.4 picometers (as opposed to 14 pm with Mask B testing). Finally, a total of five Mask C data sets were obtained. The first one (shown in Fig. 17) involved a person-in-the-loop remote alignment at each chop cycle over the duration of the 8-hour data acquisition sequence. The next day, an automated procedure for the alignment at each chop cycle was implemented, and a second 8 hour-data set was taken. Finally, on the next day, three 3-chop (as opposed to 21 chops) end-to-end data sets were acquired.

The data from these five runs were processed, and the results were quite satisfying. The rms deviation between the five data sets, averaged over the 1 meter linear stage length, was 14 picometers. This demonstrates both the stability and repeatability of the test setup.

## 8. CONCLUSIONS

The diffraction testbed has shown that the diffraction modeling codes can, indeed, model diffraction effects at the 300-400 picometer level. Furthermore, the testbed has established that such measurements are repeatable from day-to-day to 14 picometers, and that the error bars associated with any single chop diffraction measurement are 6.4 picometers. Repeatability and measurement capabilities at these levels guarantee that the SIM flight instrument can be calibrated, on orbit, to mission requirement levels. The ability of modeling codes to faithfully represent physical hardware allows one to set requirements for, and to design systems, confident in the knowledge that these codes have been validated by test.

## ACKNOWLEDGEMENT

This work was performed at the Lockheed Martin Advanced Technology Center and in part at the Jet Propulsion Laboratory, California Institute of Technology under contract with the National Aeronautics and Space Administration. The authors would like to thank Bob Korechoff of JPL for his valuable insight and comments.